JGR Solid Earth

RESEARCH ARTICLE
10.1029/2024JB030825

A ~700-km-Long Fossil Tonian Magmatic Arc Belt Hidden Within the Yangtze Block's Interior, South China

Zhidong Gu[1], Junyong Li[2], Xiaolei Wang[2], Ya Xu[3], and Xiufen Zhai[1]

[1]Research Institute of Petroleum Exploration and Development, PetroChina, Beijing, China, [2]State Key Laboratory of Critical Earth Material Cycling and Mineral Deposits, Nanjing University, Nanjing, China, [3]Key Laboratory of Deep Petroleum Intelligent Exploration and Development, Institute of Geology and Geophysics, Chinese Academy of Sciences, Beijing, China

Key Points:

- Deep boreholes and seismics reveal widespread Tonian (ca. 800 Ma) rhyolite/granites beneath the central Sichuan Basin, Yangtze Block
- High positive magnetic anomaly belt corresponds to a Tonian magmatic arc involving differentiation or reworking of basaltic magmas/rocks
- Long-distance (>400–900 km) magmatic arc migration and a broad orogenic system occurred in the Yangtze Block during Tonian period

Supporting Information:

Supporting Information may be found in the online version of this article.

Correspondence to:

Z. Gu and J. Li,
guzhidong@petrochina.com.cn;
ljy@nju.edu.cn

Citation:

Gu, Z., Li, J., Wang, X., Xu, Y., & Zhai, X. (2025). A ~700-km-long fossil Tonian magmatic Arc belt hidden within the Yangtze block's interior, South China. *Journal of Geophysical Research: Solid Earth*, *130*, e2024JB030825. https://doi.org/10.1029/2024JB030825

Received 22 NOV 2024
Accepted 22 JUN 2025

Author Contributions:

Conceptualization: Zhidong Gu, Junyong Li
Data curation: Zhidong Gu, Junyong Li, Ya Xu, Xiufen Zhai
Formal analysis: Zhidong Gu, Junyong Li, Ya Xu
Funding acquisition: Zhidong Gu, Junyong Li, Xiaolei Wang
Investigation: Zhidong Gu, Xiufen Zhai
Methodology: Zhidong Gu, Junyong Li, Xiaolei Wang, Ya Xu
Project administration: Zhidong Gu
Resources: Zhidong Gu, Ya Xu
Supervision: Zhidong Gu, Junyong Li, Xiaolei Wang
Validation: Zhidong Gu, Junyong Li, Ya Xu
Visualization: Zhidong Gu, Junyong Li, Ya Xu
Writing – original draft: Zhidong Gu, Junyong Li

Abstract Fossil magmatic arcs preserve important archives of juvenile magmatism, crustal growth and differentiation, thereby aiding in our understanding of continental evolutionary histories. However, some ancient arcs are situated in continental interiors, where they are buried beneath thick cover sequences, making their identification challenging. Here, we present a data set of deep boreholes, geochronology, geochemistry and geophysics to investigate the basement properties and evolution of the Sichuan Basin in the Yangtze Block, South China. These results provide evidence for a large Tonian magmatic arc belt hidden within the Yangtze Block's interior. Seven deep boreholes (~3,600–6,500 m) penetrating into basin basement, together with geochronology and 3D seismic reflection profiles, show extensive Tonian (ca. 820–770 Ma) rhyolite/granites overlain by Ediacaran sediments. Aeromagnetic data delineate a NE-SW-trending, ~700-km-long positive magnetic anomaly belt (PMAB) across the central basin, indicating the presence of (ultra-) mafic rocks in lower crust. Petrogenetic analyses indicate that the Tonian felsic rocks drilled within PMAB range were likely derived from a juvenile arc basaltic source. Thus, we interpret the PMAB recorded input of mantle-derived melts and their subsequent evolution into granitic magmas, associated with a Tonian arc magmatic front that once occurred in the Yangtze Block's interior. Our finding broadens the range of the Tonian continental arc system in the region, reaching at least 400–900 km landward from block's northwestern margin. Such a broad orogenic system played a vital role in continental evolution, element recycling and basin formation of the Yangtze Block.

Plain Language Summary Fossil magmatic arcs hold vital clues of how continental crust formed, grew, and evolved during Earth's history. However, some arcs are buried deep and hard to detect. This study used data from deep drilling, rock dating, geophysical imaging, and geochemical analyses to provide evidence of a hidden extinct magmatic arc beneath the Sichuan Basin, in the interior of the Yangtze Block of South China. Seven boreholes (3.6–6.5 km deep) uncovered a widespread Tonian rhyolite/granite (ca. 820–770 Ma) basement beneath the basin. Aeromagnetic surveys identified a 700-km-long positive magnetic anomaly belt (PMAB) across the central basin, reflecting the existence of (ultra-) mafic rocks in lower crust. The drilled felsic rocks from PMAB are geochemically juvenile and arc-like and show a strong mantle contribution in their source. We consider the PMAB may be associated with a Tonian magmatic arc, recording intrusion of mantle-derived basaltic melts and their evolution to felsic igneous rocks. This discovery indicates the Tonian continental arc system extended far inland, at least ~400–900 km from the Yangtze Block's northwestern margin. This wide orogenic system played a key role in shaping the Yangtze Block and element recycling within it.

1. Introduction

Continental arcs, exemplified by the modern Andes or Cretaceous Sierra Nevada batholith, are characterized by topographic high, long, and narrow regions with significant magmatic-tectonic activities along continental margins (Ducea et al., 2015; Lee et al., 2015). They are closely associated with plate subduction tectonics and act as major sites for juvenile magmatism, mantle-crust interactions, and the interplay between endogenous and exogeneous processes, thereby holding critical information on continental generation and recycling processes (Jagoutz & Kelemen, 2015; Lee et al., 2015). There is a consensus that modern-style plate tectonics have been prevailing since Neoproterozoic Era (Cawood & Hawkesworth, 2014; Stern, 2018, 2020), leading to diachronous and episodic continental arc activities at peripheries of major continents (Cao et al., 2017). However, some

Writing – review & editing: Zhidong Gu, Junyong Li, Xiaolei Wang, Ya Xu, Xiufen Zhai

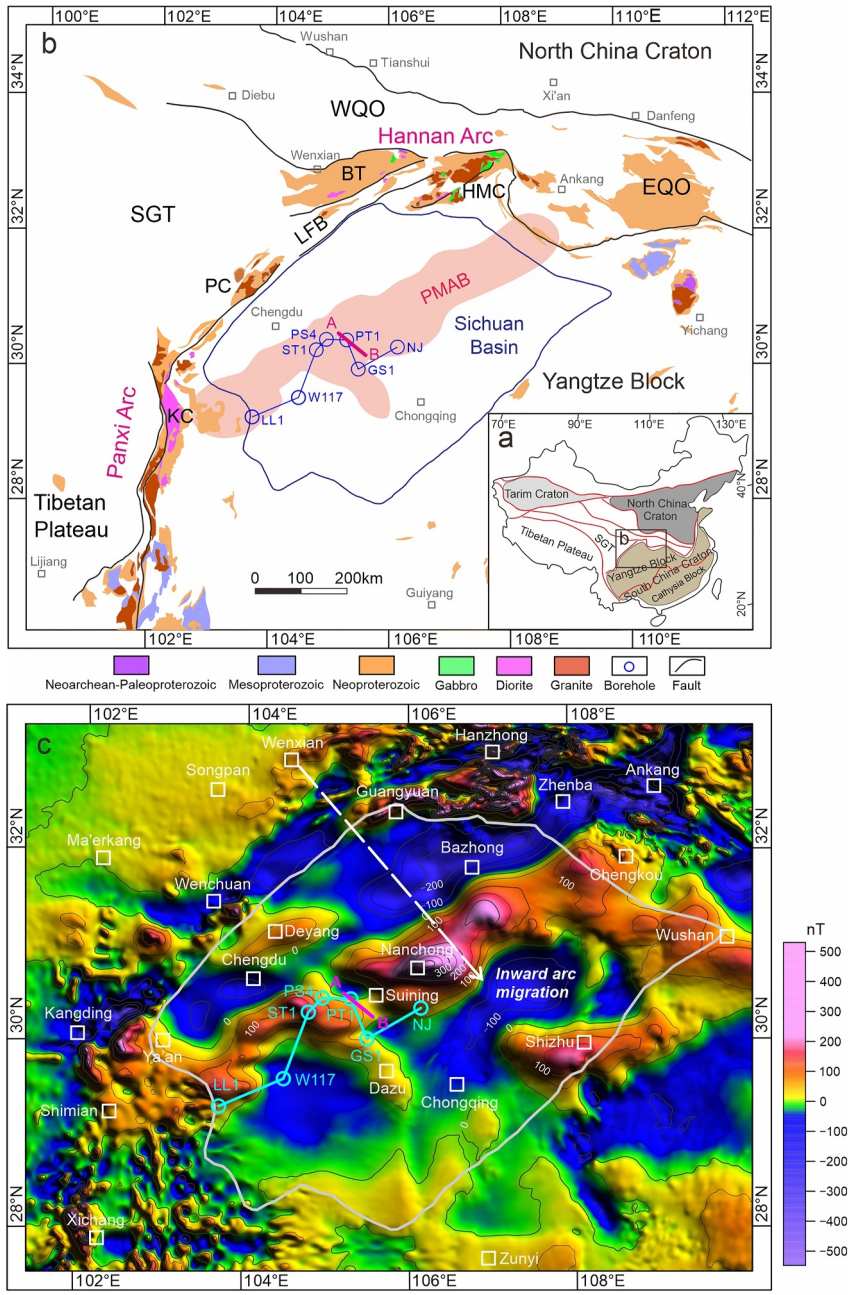

Figure 1. Simplified geological and aeromagnetic anomaly maps in the vicinity of the Sichuan Basin, NW Yangtze Block of South China. (a) Schematic tectonic map of China showing location of the Yangtze Block. SGT, Songpan-Ganzi terrane. (b) Geological map showing the distributions of Precambrian basement and the Neoproterozoic Panxi-Hannan Arc (PHA) in western-northwestern Yangtze Block. The distribution range of the high positive magnetic anomaly belt (PMAB) in the central Sichuan Basin is highlighted in pink on the map. The borehole locations (*LL1, W117, ST1, PS4, PT1, GS1,* and *NJ*) and seismic profile A-B in Figure 5 are also marked on the map. LFB, Longmenshan fold-thrust belt; BT, Bikou terrane; WQO, West Qinling orogen; EQO, East Qinling orogen; PC, Pengguan Complex; KC, Kangding Complex; HMC, Hannan-Micangshan Complex. (c) An aeromagnetic anomaly map showing the NE-SW-trending, ~700-km-long, PMAB across the central Sichuan Basin, depicted in red. In contrast, the low negative magnetic anomaly belt is represented in blue. The white dotted line indicates inferred minimum migration distance of the Tonian magmatic arc front.

ancient continental arcs, especially those in continental interiors distant from continental margins, are often less exposed at the surface due to later thick sedimentary cover. Identifying and reconstructing these fossil intra-continental arcs are essential for understanding continental evolutionary histories.

The Yangtze Block in the northwestern part of South China Craton (Figure 1a) experienced extensive and prolonged oceanic subduction around its periphery during Tonian period, which promoted significant crustal growth and reworking of the block (Dong et al., 2024; Shu et al., 2021; Xiong et al., 2023; Zhao & Cawood, 2012; Zhao et al., 2011). Its western–northwestern margin is characterized by a continuous belt of subduction-related igneous rocks extending over 1,000 km—primarily calc-alkaline intrusive rocks—known as the Panxi-Hannan Arc (PHA; Figure 1b) (Zhao & Cawood, 2012; Zhao et al., 2021; Zhou, Yan, et al., 2002). Available data indicate the PHA dominantly formed during ca. 880–750 Ma (Tonian period) and represents an extinct continental arc in Earth's history (Dong et al., 2024; Zhao et al., 2018). However, the spatial distribution of this ancient continental arc system remains enigmatic, particularly regarding whether a contemporaneous arc counterpart exists within the block's interior.

In this study, we take advantage of newly-acquired geophysical and deep boreholes data from the Sichuan Basin to investigate the basement characteristics of the Yangtze Block's interior, South China (Figure 1b). We find an extensive fossil Tonian magmatic arc possibly buried beneath the Sichuan Basin. We then reconstruct the Tonian trans-Yangtze Block continental arc system and discuss its effects for the initial subsidence and sedimentation of the Sichuan Basin.

2. Geological Background

The Yangtze Block of South China is tectonically separated from the North China Craton to the north, from the Songpan-Ganzi terrane and Tibetan Plateau to the west, and the Cathaysia Block to the southeast. During Neoproterozoic Era, the Yangtze Block occupied exterior locations of Rodinia supercontinent, where it experienced prolonged subduction of the exterior oceanic lithosphere, leading to significant crustal growth and reworking (Cawood et al., 2018; Dong et al., 2024; Li et al., 2024; Shu et al., 2021; Wu et al., 2023; Xiong et al., 2023). Correspondingly, its southeastern margin, delineated by the Jiangnan Orogen, experienced accretionary orogenesis since ca. 970 Ma and may have amalgamated with the Cathaysia Block by ca. 810 Ma (e.g., Shu et al., 2021; Wang et al., 2014; Yao et al., 2019). However, other studies propose that final amalgamation between Yangtze and Cathaysia blocks may not occur until Ordovician (e.g., Lin et al., 2023; Wang et al., 2023). On the other hand, the western-northwestern margin of the Yangtze Block represents a Neoproterozoic subduction zone that recorded active tectonic-magmatic processes at least from ca. 970 to 750 Ma (Li et al., 2024): it commenced with intra-oceanic arc regime before ca. 970 Ma (Li et al., 2018) and then transitioned to continental arc regime since ca. 870 Ma (Zhao et al., 2018). This continental arc regime persisted over 100 Myr and was characterized by high magmatic flux (Dong et al., 2024; Xiong et al., 2023). Since the Mesozoic, large volumes of Neoproterozoic igneous and metamorphic rocks in the region have been uplifted to the surface due to extrusion and thrusting processes associated with the Mesozoic collision between North China and South China cratons, as well as Cenozoic India-Eurasia convergence (Wang & Meng, 2009). These rocks are primarily preserved as linearly-distributed metamorphic-plutonic complexes (e.g., the Hannan-Micangshan,Pengguan, Kangding complexes; see Figure 1b) within the PHA belt.

The Sichuan Basin, located in the northwestern Yangtze Block (Figure 1b), is an ancient and long-lived (>635 Ma) cratonic basin (Gao et al., 2016; Gu et al., 2021; Korsch et al., 1991). It experienced multiple tectonic cycles and deposited sedimentary successions up-to-10 km thick since the Cryogenian or Ediacaran period, including Cryogenian diamictite-bearing units, Ediacaran to Middle Triassic marine carbonate rocks, and Late Triassic to Quaternary terrigenous siliciclastic rocks (Gu et al., 2021; L. Liu et al., 2021; S. G. Liu et al., 2021). The Sichuan Basin is currently surrounded by mountain belts as a result of Late Triassic to Cenozoic orogeny (L. Liu et al., 2021; S. G. Liu et al., 2021). As hydrocarbon exploration advanced, numerous deep boreholes were drilled in the central basin over the past decade, some of which have penetrated into the basin basement (Figures 1b and 1c). These deep boreholes are important to uncover the characteristics of basin basement beneath the thick sedimentary cover.

3. Data and Methods

3.1. Data

To investigate the characteristics of the basin basement, we conducted a comprehensive analysis of deep boreholes, aeromagnetic anomaly and 3D seismic data. We collect six granites, five rhyolites, and five rhyolites from

deep borehole cores of *W117*, *PT1*, and *NJ*, respectively. The aeromagnetic data was compiled by the Airborne Geophysical Remote Sensing Center of the Ministry of Land and Resources of China, which was gridded with 2 km interval. Furthermore, the 3D seismic data in the central Sichuan Basin were collected by China National Petroleum Corporation (CNPC). These seismic data are of positive polarity, with black events representing positive amplitudes in the seismic sections.

All geophysical and geochemical data acquired in this study are novel and have not been previously reported, except for the zircon U-Th-Pb isotopic data of *W117-264* granite (n = 15), which are sourced from Gu et al. (2014).

3.2. Methods

3.2.1. Curie Point Depths Estimation by Aeromagnetic Data

The Curie point depth (CPD) can reflect the deep crustal structure and its thermal state. The spectral method is the most widely used technique to estimate CPD. Under the assumption that the magnetized layer extends infinitely far in all directions and the magnetization is a random function, the radial average of the power-density spectrum of the total magnetic field anomaly can be expressed as a function of the top and bottom of the magnetic layer (Tanaka et al., 1999). The power-density spectrum of the total magnetic field anomaly can be expressed as:

$$\overline{\Phi}_{\triangle T}(|k|) = Ae^{-2|k|z_t}\left(1 - e^{-|k|(z_b - z_t)}\right)^2 \quad (1)$$

where k is the radial wavenumber, Z_t and Z_b are the top and bottom of the magnetic layer respectively, and A is a constant.

For wavelengths less than about twice the thickness of the layer, the top bound of the magnetic layer can be estimated by the slope of the logarithm of the power spectrum of the total field anomaly at medium to high wavenumbers. At long wavelengths, the centroid of the magnetic layer can be estimated based on the logarithm of the ratio between the power spectrum of the total field anomaly and the wavenumbers. Therefore, the bottom of the magnetic layer, the CPD, can be estimated.

The power-density spectrum of aeromagnetic data in the Sichuan Basin was calculated with a window size of 100 × 100 km, the sliding step of the window is 80 km to keep 20 km overlap of each window. The top and the centroid depth of the magnetic layer were calculated from the spectrum in each window. The final CPD result was obtained and shown in Figure S1 of Supporting Information S1. The uncertainty of the CPD can be estimated from the fitting error of the top and centroid depth estimation. As the CPD is derived by deducting the top depth of the magnetic layer from twice of the centroid depth, the uncertainty of CPD is generally less than 1 km (Figure S2 in Supporting Information S1).

3.2.2. Zircon Geochemistry

Zircon U-Th-Pb-Hf-O isotopic and trace elemental analyses were performed with the aid of guidance of cathodoluminescence (CL) images, as well as transmitted and reflected photographs, to avoid analytical domains with cracks, inclusions, or heterogeneous luminescenece. Zircon U-Th-Pb isotope analyses for sample NJ, along with zircon O isotopes and trace elements for all samples, were conducted on a Cameca IMS-1300HR^3 secondary ion mass spectrometry (SIMS) at the State Key Laboratory of Critical Earth Material Cycling and Mineral Deposits in Nanjing University (CEMYMD-NJU). The instrument conditions and detailed procedures followed those outlined by Li et al. (2024). Secondary standard reference (i.e., Qinghu zircon) was used to monitor U-Pb dating and O isotopic results. Four measurements of the Qinghu zircon standard yielded a weighted mean $^{206}Pb/^{238}U$ age of 161 ± 2 Ma (2σ; MSWD = 0.42), consistent with its recommended value of 159 ± 0.2 Ma (Li et al., 2013). Twenty measurements of the Qinghu zircon standard yielded a weighted mean $\delta^{18}O$ value of 5.6 ± 0.26 ‰ (2σ), consistent with the reported value of 5.4 ± 0.2‰ (2σ) (Li et al., 2013). Trace elemental concentrations were standardized against the zircon standard 91,500 (Table 3 in Coble et al., 2018), which yields relative standard deviations of ± 2%–5% for U and Th, ± 1%–4% for Ti, ± 4%–10% for Hf, ± 2%–7% for Y and HREEs. Zircon Lu–Hf isotopic analysis was conducted using a GeoLas 193 nm laser-ablation system attached to a Neptune (Plus) MC-ICP-MS at the CEMYMD-NJU. The detailed experiment and data reduction procedures followed those outlined by Li et al. (2024). Reference zircon Mud Tank were used to monitor accuracy and precision of Hf

isotope ratios and instrumental drift with respect to the Lu/Hf ratios. The obtained $^{176}Hf/^{177}Hf$ ratios were 0.282,499 ± 0.000026 (n = 25; 2σ) for Mud Tank, and were consistent with the recommended value (0.282507 ± 0.000006; Woodhead & Hergt, 2005).

Zircon U-Th-Pb isotope analyses for sample PT1 rhyolite and W117-311 granite were conducted on a sensitive high-resolution ion microscope (SHRIMP) at the Beijing SHRIMP Center, the Institute of Geology, Chinese Academy of Geological Sciences. The critical operating conditions included 5-scan duty cycle, 4.5 nA and 10 kV primary O^{2-} beam, and mass resolution ~5,000. The method of SHRIMP U-Pb dating was given in detail by Yan et al. (2003) and Druschke et al. (2006). About 15–20 zircon grains were dated for each sample. Zircon standard SL13 (U = 238 ppm, reference age of 572 Ma) was used for calibrating the U contents, and zircon standard TEMORA ($^{206}Pb/^{238}U$ = 0.0668, reference age of 417 Ma) was used for calibrating the $^{206}Pb/^{238}U$ ratios.

3.2.3. Whole-Rock Major and Trace Elements

Major and trace elemental composition for borehole samples were analyzed at the Analytical Laboratory, Beijing Research Institute of Uranium Geology. All the samples were firstly powdered by using an agate mortar. The Loss on ignition (LOI) values were obtained by measuring the weight loss after heating sample powders at 980°C. Major elements were measured using an Xray fluorescence spectrometer (XRF), by testing well-mixed glass disks which were made by high-temperature fusion of samples powders and lithium metaborate flux. Two national standards (basalt GBW07105, soil GBW07107) were simultaneously analyzed to monitor the analytical quality. The analytical precision (RSD) for most elements is less than 3 wt%, except for MnO, which is below 5 wt%. Trace elements were analyzed using an Inductively Coupled Plasma Mass Spectrometer (ICP-MS). Before ICP-MS measurement, sample powders were completely dissolved by Hf–HNO_3–$HClO_4$ mixture acid solutions and diluted with 1% HNO_3. Two national standards (andesite GBW07104 and stream sediments GBW07312) were used to monitor the instrument performance. The analytical uncertainties were better than 5% for most trace elements, except for Be, Cd, In, and Sb.

4. Results

4.1. Aeromagnetic Anomaly Map

Figure 1c presents a high-resolution aeromagnetic anomaly map of the Sichuan Basin and its surrounding areas. This map displays magnetic field intensity values ranging from about −550 to 500 nT (nano tesla) and illustrates a heterogeneous deep-crustal composition beneath the basin. Key features of the map include a stripe-shaped, NE-SW-trending, and continent-margin-parallel high positive magnetic anomaly belt (PMAB; magnetic field intensity value > 0) and the low negative magnetic anomaly belt (NMAB; magnetic field intensity value < 0). The PMAB at the basin's exterior region (i.e., the PHA) generally relates to Tonian plutonic complexes that are exposed at surface, including the Kangding, Pengguan, and Hannan-Micangshan Complexes (Figure 1b). These plutonic complexes predominantly consist of calc-alkaline intermediate to felsic plutons, which are closely associated with mafic-ultramafic intrusions (Li et al., 2024; Zhao & Cawood, 2012; Zhao et al., 2019, 2021). Within the interior of the Sichuan Basin, the PMAB prominently extends in a SW-NE direction, spanning ~700 km in length and >50 km in width, covering a ~53,000 km^2 distribution area (Figures 1b and 1c). It is delineated from the NMAB by a straight NW boundary and a curved SE boundary (Figure 1c). The PMAB indicates the presence of a buried, predominantly (ultra-) mafic rock belt beneath the basin, given the magnetic minerals, such as magnetite, commonly found in mafic and ultramafic rocks. Additionally, the maximum Curie point depth (CPD) for the (ultra-) mafic rock belt is estimated to be 16–20 km (relatively lower crustal levels) according to aeromagnetic data (Figure S1 in Supporting Information S1). In contrast, the NMAB usually reflects a predominantly meta-sedimentary and/or felsic rock belt beneath the basin, which typically contain fewer iron-rich minerals like magnetite.

4.2. Deep Boreholes

There are seven deep boreholes penetrating into the basement within the central Sichuan Basin to unravel the basement characteristics (locations shown in Figures 1b and 1c). The stratigraphic correlations of these boreholes are detailed in Figure 2a. Notably, the lowermost stratigraphic/magmatic sequences for the borehole *W117* and borehole *LL1* consist of granite and a granite-diorite-syenite association, respectively (Figures 2a, 2b and 3a–3c). The other five boreholes (*ST1, PT1, PT4, GS1,* and *NJ*) have rhyolites as the main rock type of the basal rock

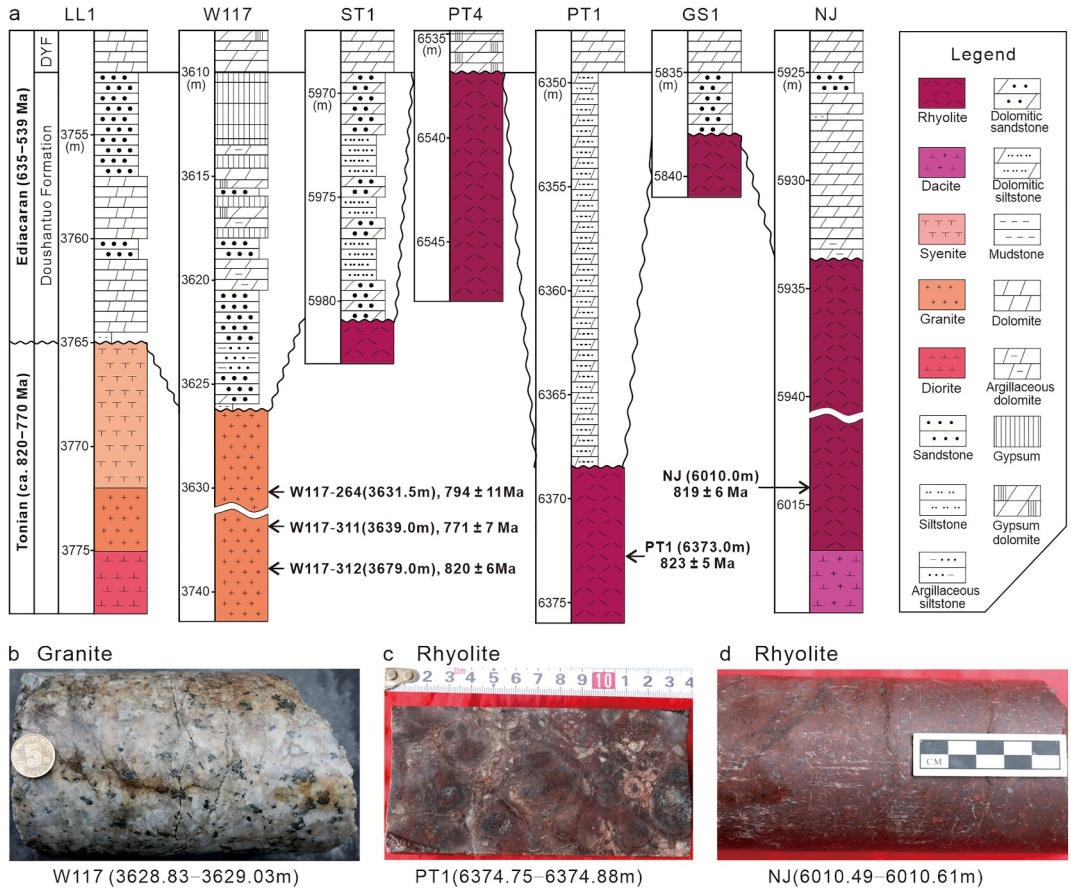

Figure 2. Stratigraphic correlation column of boreholes penetrating into the basement of the Sichuan Basin and typical hand specimen photographs of collected Tonian rhyolite/granite cores. (a) Stratigraphic correlation column from deep boreholes within the central Sichuan Basin. (b–d) Representative hand specimen photographs of collected Tonian rhyolite/granite cores from boreholes *W117*, *PT1*, and *NJ* respectively. DYF, Dengying Formation.

sequences (Figures 2a–2d, and 3d–3f). Precise zircon U-Pb dating results constrain the rhyolite/granites of ca. 820–770 Ma (Figures 2a and 4). And all rhyolite/granites are unconformably overlain by the Ediacaran (635–539 Ma) carbonate and siliciclastic rocks (Figure 2a). This unconformity represents a significant temporal gap of over 140 Myr and is interpreted to result from regional uplift and exhumation during Tonian to Cryogenian periods (770–635 Ma), prior to the Ediacaran period.

4.3. 3D Seismic Interpretation

A substantial data set of high-quality 3D seismic data from the central Sichuan Basin is utilized to delineate the basement features (Figure 5; Figures S4–S6 in Supporting Information S1). The seismic profiles show overall horizontal strong reflections within the basement. However, a series of low-angle, strong seismic reflections are observed just below the Ediacaran System. These reflections extend downward into the lower basement and are truncated at a low angle by the overlying Ediacaran strata (Figure 5, Figures S4 and S5 in Supporting Information S1). The distribution of these low-angle seismic reflections is extensive across the central Sichuan Basin and falls within the PMAB area (Figure S6 in Supporting Information S1). Most previous studies interpreted them as extensional faults before the drilling of deep boreholes into the basin basement (e.g., Gu & Wang, 2014; Guan et al., 2017; Yang et al., 2014).

In this study, we consider these reflections may represent fossilized magma ascent conduits (Figure 5) rather than extensional faults by following lines of evidence. Firstly, the ultra-deep borehole *PT1*, which penetrates eight m into the basement and intersects one of these low-angle reflections (Figure 5), confirms that these reflections are associated with rhyolites (Figures 2a and 2c). Accordingly, we infer that the low-angle, strong seismic reflections

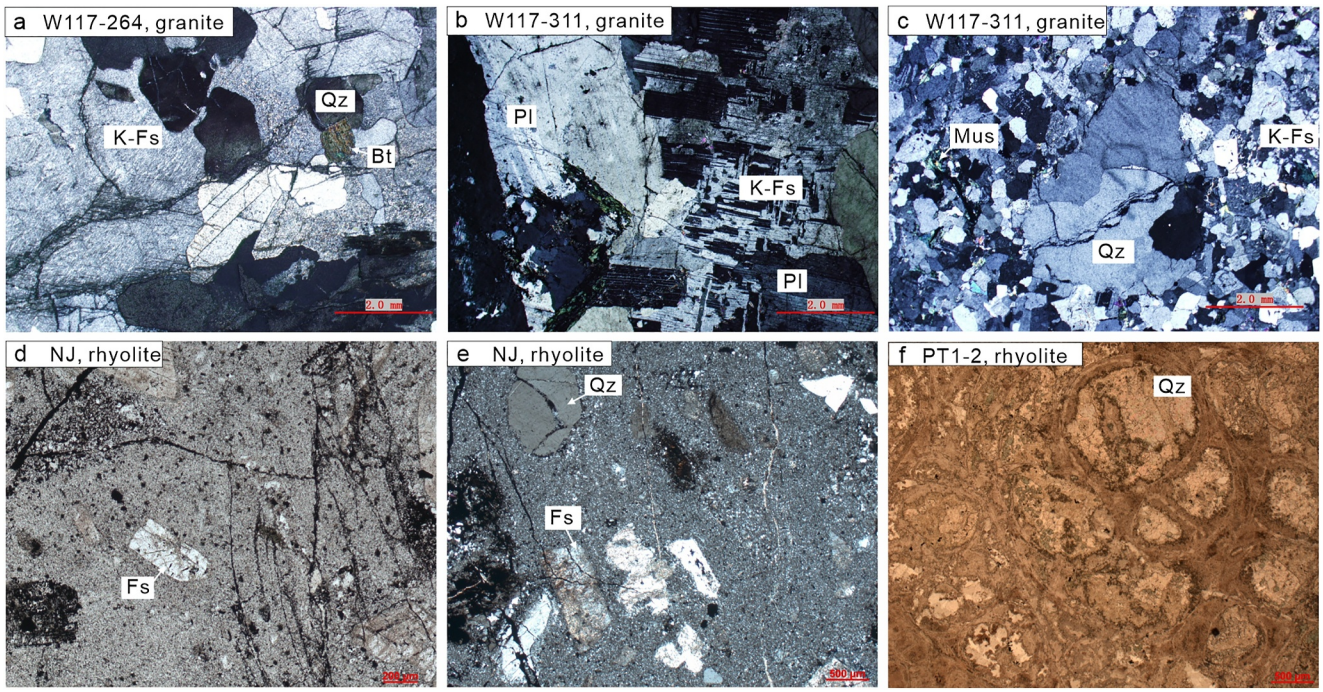

Figure 3. Photomicrographs of representative granites and rhyolites from deep borehole cores (a–c) Granites from borehole *W117*. (d–f) Rhyolites from boreholes *NJ* and *PT1*. K-Fs, K-feldspar; Qz, quartz; Bt, biotite; Pl, plagioclase; Mus, muscovite.

correspond to volcanic or intrusive rocks, given that igneous rocks typically exhibit distinct seismic impedance values—such as velocity and density—compared to surrounding meta-sedimentary rocks. Secondly, the structures of extensional faults are not clear in the seismic profiles, because it is difficult to identify clear hanging wall and its corresponding footwall strata adjacent to these low-angle, strong reflectors. Thirdly, the indicators of crustal extension such as block rotation and wedge-shaped syn-tectonic sedimentary fills near the low-angle reflectors are also absent. In this regard, we suggest these magma ascent conduits may once connect upper crustal magma reservoirs to deeper (ultra-)mafic sources. And their widespread occurrence beneath the basin suggests a potential genetic link between the (ultra-) mafic rocks at lower crustal levels and the felsic igneous rocks at upper crustal level.

4.4. Geochemistry and Petrogenesis for Drilled Cores

All samples from collected cores are relatively fresh, given (a) the secondary minerals are sporadically present in the samples, and (b) the plagioclase grains within samples exhibit clear compositional zoning and limited alteration (Figure 3). Geochemically, they are primarily metaluminous–slightly peraluminous (A/CNK = 0.88–1.13) and evolved, characterized by high silica (SiO_2 = 68.0–76.0 wt%) and alkali ($Na_2O + K_2O$ = 7.5–9.6 wt%), but low calcium (CaO = 0.2–1.5 wt%) and alumina (Al_2O_3 = 11.1–13.8 wt%) contents (Figure S7, Table S1 in Supporting Information S1). In the primitive-mantle normalized trace elemental diagrams, they are enriched in large ion lithospheric elements (e.g., Rb and K) and depleted in Nb, Ta, and Ti (Figure S8 in Supporting Information S1).

In order to explore the petrogenesis of the collected Tonian rhyolite/granites, we utilized detailed analyses on zircon U-Pb-Hf-O isotopes and trace elements. Zircon typically crystallizes and partitions elements from felsic melts, which permits determination of (a) the timing of crystallization and (b) the compositional evolution and source of the magma from which it grew (Ge et al., 2023; Kemp et al., 2007; Roberts et al., 2024; Tang et al., 2021; Valley, 2003). For example, zircon Hf isotopes can reveal whether the host magma originated from a juvenile source, and enriched continental source, or a mixture of both (Kemp et al., 2007). Zircon O isotopes can record whether supracrustal or hydrothermally altered materials were involved during the formation of the host rock (Valley, 2003). Zircon U/Yb and Ce/U ratios can reflect potential assimilation of sediments or fluid effect during formation of the host magma (Grimes et al., 2015; Roberts et al., 2024).

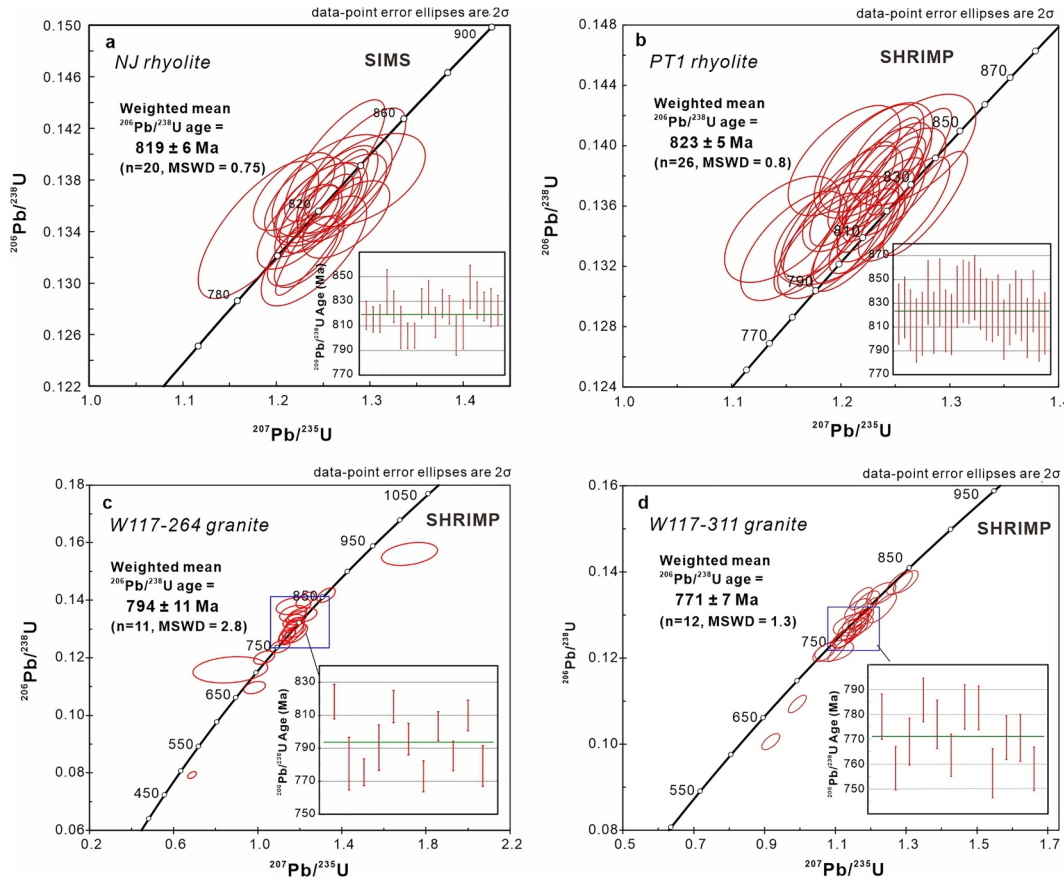

Figure 4. Zircon U-Pb dating results. (a) Weighted mean $^{206}Pb/^{238}U$ age of 819 ± 6 Ma for the borehole *NJ* rhyolite by secondary ion mass spectrometry method. (b) Weighted mean $^{206}Pb/^{238}U$ age of 823 ± 5 Ma for the borehole *PT1* rhyolite by SHRIMP method. (c–d) Weighted mean $^{206}Pb/^{238}U$ ages of 794 ± 11 (Gu et al., 2014) and 771 ± 7 Ma for the borehole *W117* granites by SHRIMP method. Zircon cathodoluminescence images and measured spots for U-Pb-O-Hf and trace elements can be found in Figure S3 in Supporting Information S1.

Zircons in rhyolite/granites from three boreholes show similar U-Pb crystallization ages (i.e., ca. 820–770 Ma; Figure 4), REE (rare earth element) patterns, and Th/U ratios of mostly >0.3 that are indicative of magmatic origins (Table S2 in Supporting Information S1). However, the drilled rhyolite/granites from the PMAB and NMAB areas show distinct zircon Hf-O isotopic compositions and trace elemental ratios (e.g., Ce/U, U/Yb) (Figure 6), hinting at their different petrogenesis. The variations in zircon Hf-O isotopes among the samples are likely controlled primarily by their different magmatic source compositions, as both the PT1 rhyolite from the PMAB and W117 granites from the NMAB are highly evolved in whole-rock compositions and do not exhibit clear magmatic evolutional relationships (Figures S7, S8 in Supporting Information S1).

For the *PT1* and *NJ* rhyolites from the PMAB area, their formation was likely linked to differentiation or rapid reworking of mantle-derived basaltic melts/rocks within a continental arc setting, as supported by the following lines of evidence. Firstly, zircons from these rhyolites consistently display high Th/U and Ce/U ratios (Figure 6b), and homogeneous high $\varepsilon_{Hf}(t)$ values (+3.7 to +9.0) (Figure 6a), suggesting a juvenile source for the magma with minor influence of sedimentary materials during its formation (Roberts et al., 2024). Secondly, the majority of zircons show geochemical similarities (e.g., U/Yb and Hf concentrations) with zircon from known continental arc rocks (Figures 6c and 6d; Grimes et al., 2015). Thirdly, we employed Eu/Eu*-in-zircon (Tang et al., 2021) proxy to evaluate the crustal thickness where boreholes *PT1* and *NJ* rhyolites formed. The *PT1* rhyolites are high in silica (SiO_2 > 75 wt%) and do not meet the calculation criterion for this proxy (Tang et al., 2021). In contrast, the *NJ1* rhyolites, being I-type with lower silica contents (SiO_2 < 70 wt%), are suitable for calculation. Twenty zircons from *NJ1* sample yielded an estimated crustal thickness of 39.9 ± 2.3 km (n = 20; 2SE). Given that Eu/

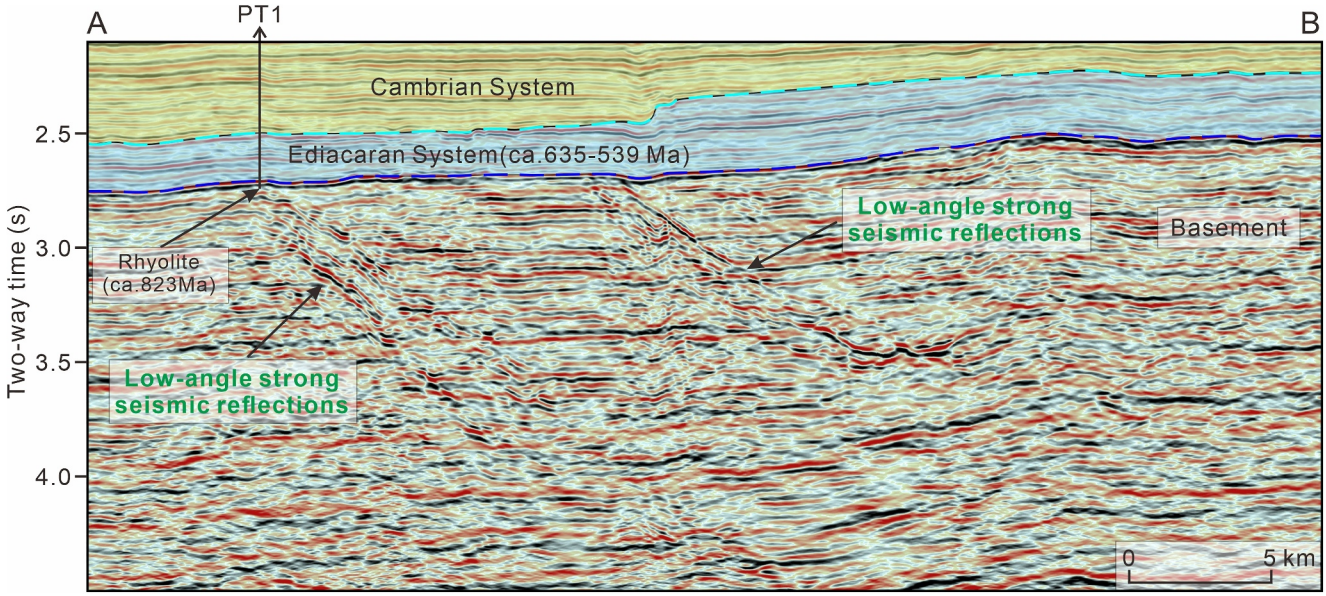

Figure 5. 3D seismic profile A-B across the borehole PT1 in the central Sichuan Basin (location shown on Figures 1b and 1c). The profile shows two sets of low-angle strong seismic reflections just below the Ediacaran System, one of which was drilled by the borehole PT1 and demonstrated to be composed of rhyolites. The seismic profile is shown at approximately a horizontal to vertical scale of 3:8.

Eu*-in-zircon and whole-rock La/Yb (Profeta et al., 2015) proxies are expected to be mutually correlated when applied to I-type igneous rocks (Tang et al., 2021), we additionally employed the whole-rock La/Yb proxy for *NJ1* rhyolites. This method yielded a crustal thickness estimation of 45.5 ± 4.6 km (n = 5; 2SE), consistent with the thickness using the zircon proxy. This consistency enhances the reliability of the crustal thickness estimation derived from the zircon Eu/Eu* proxy and suggests a thickened Tonian continental crust in the PMAB area. Overall, we suggest the PMAB area may record significant juvenile magmatism during Tonian period, characterized by melting of mantle, the input of parent mafic magmas into the lower crust, followed by their trans-crustal magmatic differentiation or rapid partial melting of lower crust, ultimately resulting in the generation of granitic melts in upper crust (Figure 7).

Regarding borehole *W117* granites from the NMAB area, their zircons mostly fall within the hybrid S-type region on the plot depicted in Figure 6a, indicating the involvement of sediments during granite formation. The *W117* zircons exhibit a range of $\varepsilon_{Hf}(t)$ values from −3.0 to +5.8 and elevated $\delta^{18}O$ values (6.6–10.8 ‰, mostly ∼10 ‰) (Figure 6b). Given that high $\delta^{18}O$ is a diagnostic signature of low-temperature water-rock interaction at Earth's surface, we suggest the sources of granites are primarily supracrustal sediments that have undergone some degree of chemical weathering and O isotope exchange. The transportation of supracrustal sediments to deep crust for partial melting may be facilitated by thrust faults (Figure 7), which are extensively developed within orogenic systems (Ducea & Chapman, 2018). A similar Tonian supracrustal recycling process has been documented in the Pengguan Complex within the PHA (Li et al., 2021). This endogenic process may represent an important mechanism for the formation of high-$\delta^{18}O$ granitic melts. Overall, we propose that the NMAB area predominantly records crustal reworking in relatively lower crust and emplacement of granitic melts in upper crust during Tonian period (Figure 7). There was limited to no contribution from mantle-derived melts in the magmatic process in the NMAB area.

5. Discussion and Implication

Based on above geophysical and geochemical results, we conclude that although both PMAB and NMAB areas of the basin contain Tonian felsic igneous rocks in upper crust, they have distinct lower-crustal compositions and underwent different magmatic processes during Tonian period. Specifically, the observed PMAB within the basin may be associated with a juvenile Tonian magmatic arc, recording the intrusion of mantle-derived basaltic melts at lower crustal levels and the emplacement of their derived granitic melts in upper crust (Figure 7). The addition of basaltic melts into the crust contributed to regional crustal growth and thickening. This fossil Tonian magmatic

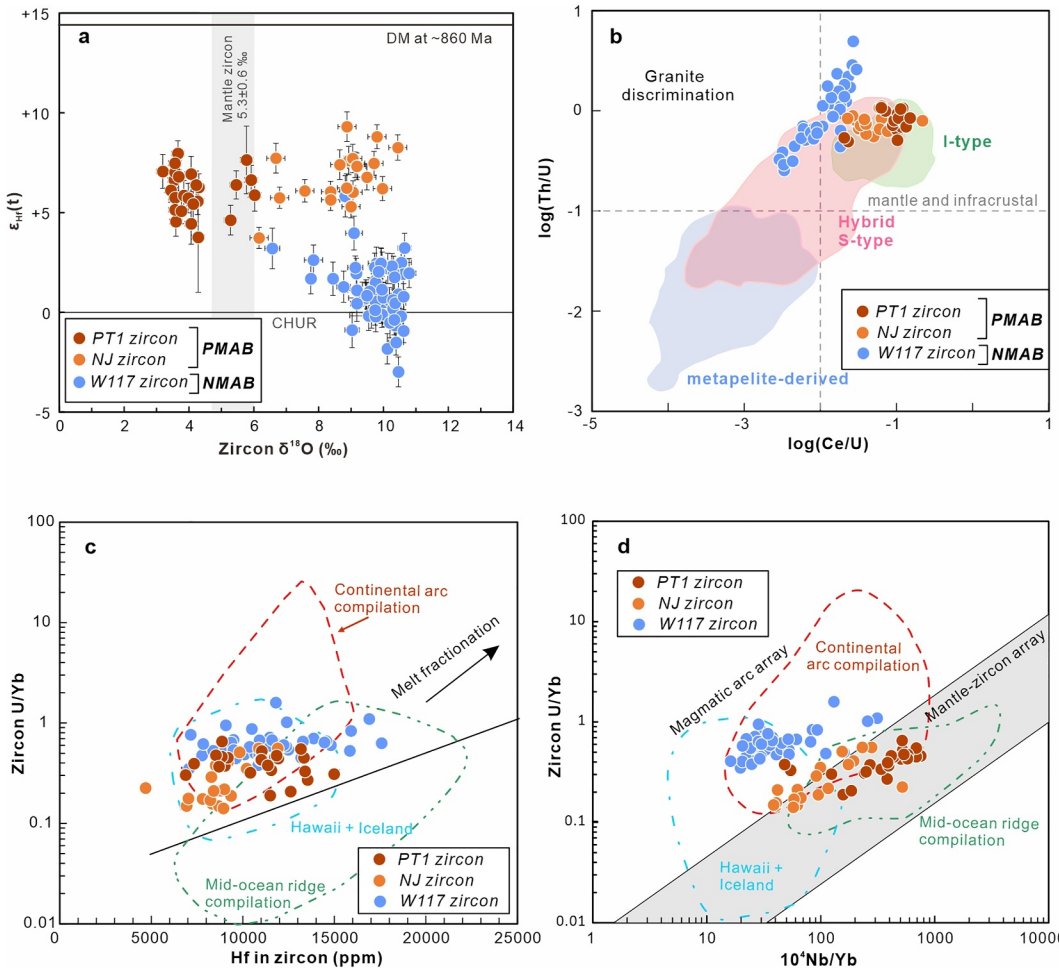

Figure 6. Isotopic and trace element composition diagrams of zircons from collected borehole Tonian rhyolite/granites cores. The PT1 and NJ samples were drilled from positive magnetic anomaly belt area, while the W117 samples were drilled from negative magnetic anomaly belt area. (a) Zircon $\varepsilon_{Hf}(t)$- $\delta^{18}O$ diagram showing the distinct isotopic compositions of zircons from three samples. (b) Zircon log(Th/U) versus log(Ce/U) (base 10) plot (after Roberts et al., 2024) (c–d) U/Yb versus Hf and 10^4*(Nb/Yb) plots for zircons from three boreholes cores. The reference fields are from Grimes et al. (2015).

arc crust, as indicated by the PMAB, should be widely distributed (i.e., mainly NE-SW-trending, nearly 700 km length, >50 km width) beneath the central Sichuan Basin (Figure 1b). A large-scale mantle input during Tonian period is also evidenced by surface exposures around the Sichuan Basin (Wu et al., 2024), exemplified by the Beiba-Wangjiangshan-Bijigou layered mafic-ultramafic intrusions, which cover an area of over 750 km^2 (Wang et al., 2016; Zhao & Zhou, 2009; Zhou, Kennedy, et al., 2002). In addition to the Sichuan Basin, similar conclusions that the PMAB is related to buried magmatic arc have been drawn for several other intracontinental basins (e.g., Garrett, 1990; He et al., 2013; Xiao et al., 2018). A representative example is the Junggar Basin in northwestern China, where the possible existence of several oroclinal magmatic arc belts beneath the basin has been supported by both zircon isotopes and seismic data (He et al., 2013; Xiao et al., 2018; Yang et al., 2022). On the other hand, the observed NMAB within the Sichuan Basin more likely documented reworking of supracrustal materials with high-$\delta^{18}O$ and more unradiogenic Hf isotopic signatures during Tonian period, leading to the formation of granitic melts (Figure 7).

A critical question pertains to whether the PMAB in the basin could alternatively relate to the back-arc section of the PHA or the Tonian continental rift, as both tectonic regimes involve a significant influx of mantle-derived melts. If this were the case, Tonian magmatism in the basin would be expected to occur in extensional

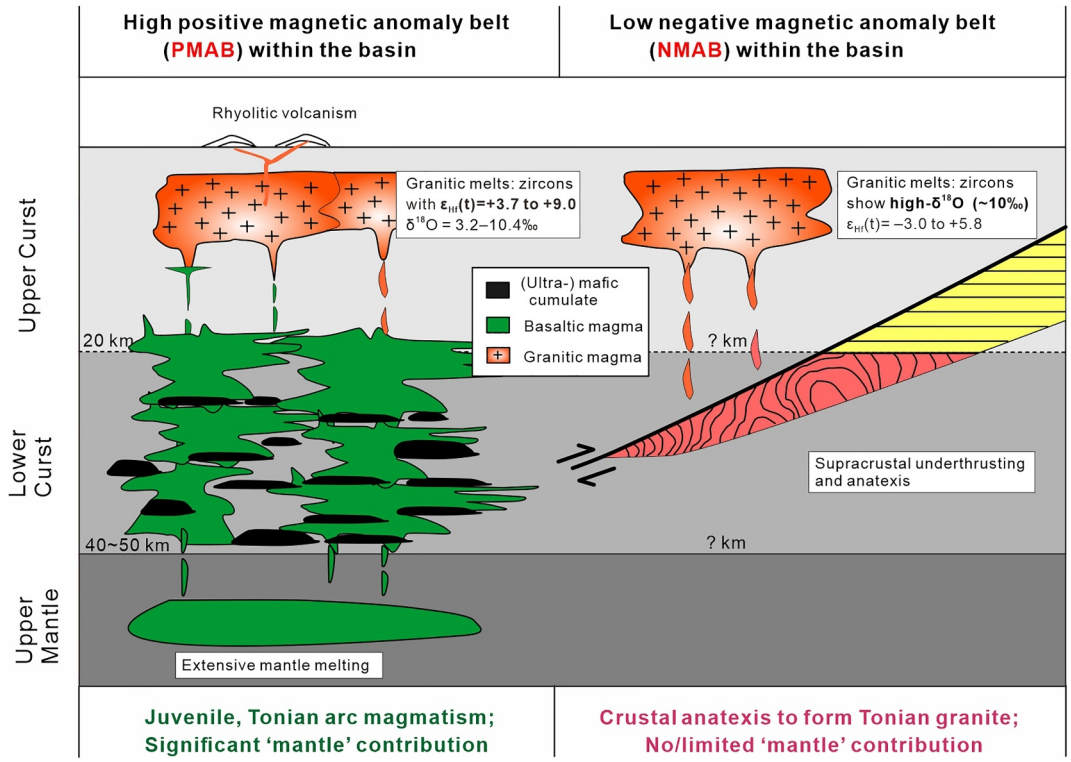

Figure 7. Cartoon shows different lower-crustal components and magmatic processes that generated granitic magmas during Tonian in positive magnetic anomaly belt (PMAB) and negative magnetic anomaly belt (NMAB) areas of the Sichuan Basin, Modified from Jacob and Moyen (2021). The PMAB area was dominated by a juvenile arc crust with significant mantle contribution during Tonian period. The Tonian felsic igneous rocks in PMAB area may represent differentiated or rapid reworking products of deeper mantle-derived basaltic melts/rocks. In contrast, the Tonian magmatism operating in the NMAB area was primarily driven by partial melting of crustal materials with high $\delta^{18}O$ and relatively unradiogenic Hf isotopes, with limited or no mantle contribution.

tectonic setting, accompanied by a thick sedimentary succession from Tonian to Cryogenian period. However, data from seven boreholes and 3D seismic profiles in this study demonstrate that the granite/rhyolite rocks (ca. 820–770 Ma) are uncomfortably overlain by the Ediacaran sedimentary successions (ca. 635–539 Ma) (Figures 2a and 5), implying a long-timescale (~140 Myr) sedimentary hiatus prior to the Ediacaran. This suggests a tectonic history more consistent with compressional regime and crust uplift, rather than extensional regime. Besides, as aforementioned, the extensional structure is not fully supported by the 3D seismic interpretation. Moreover, this study suggests that the Tonian high-$\delta^{18}O$ granites beneath the basin are genetically linked to supracrustal underthrusting that supports a compressional regime. In addition to the question posed above, another key issue is whether the PMAB in the basin corresponds to mafic–ultramafic rocks of Permian ages, rather than those of Tonian ages. This hypothesis arises from the widespread distribution of Permian mafic–ultramafic rocks in the basin's exterior regions, especially to the southwest, as exemplified by the Emeishan large igneous province (Chung & Jahn, 1995; Xu et al., 2001). However, extensive drilling (over 2,000 boreholes) through the Permian strata in the Sichuan Basin has shown that the thickness and distribution of Permian basaltic rocks progressively decrease from southwest to northeast (Chen et al., 2022; Xu et al., 2007). Within the PMAB area, most boreholes reveal the absence of Permian basaltic rocks, suggesting that these rocks cannot account for the high positive magnetic anomalies observed in the central basin.

Regionally, our findings extend the circum-Yangtze Tonian continental arc system (e.g., PHA) into the Yangtze Block's interior and provide new insights into the Tonian tectonic-magmatic evolution in the area. Similar to the PHA, we suggest the magmatic arc beneath the central Sichuan Basin is also related to southeastward oceanic subduction along the northwestern margin of the Yangtze Block. This interpretation is supported by (a) the straight northwestern boundary of the PMAB in the central basin, which is more likely to be perpendicular to the

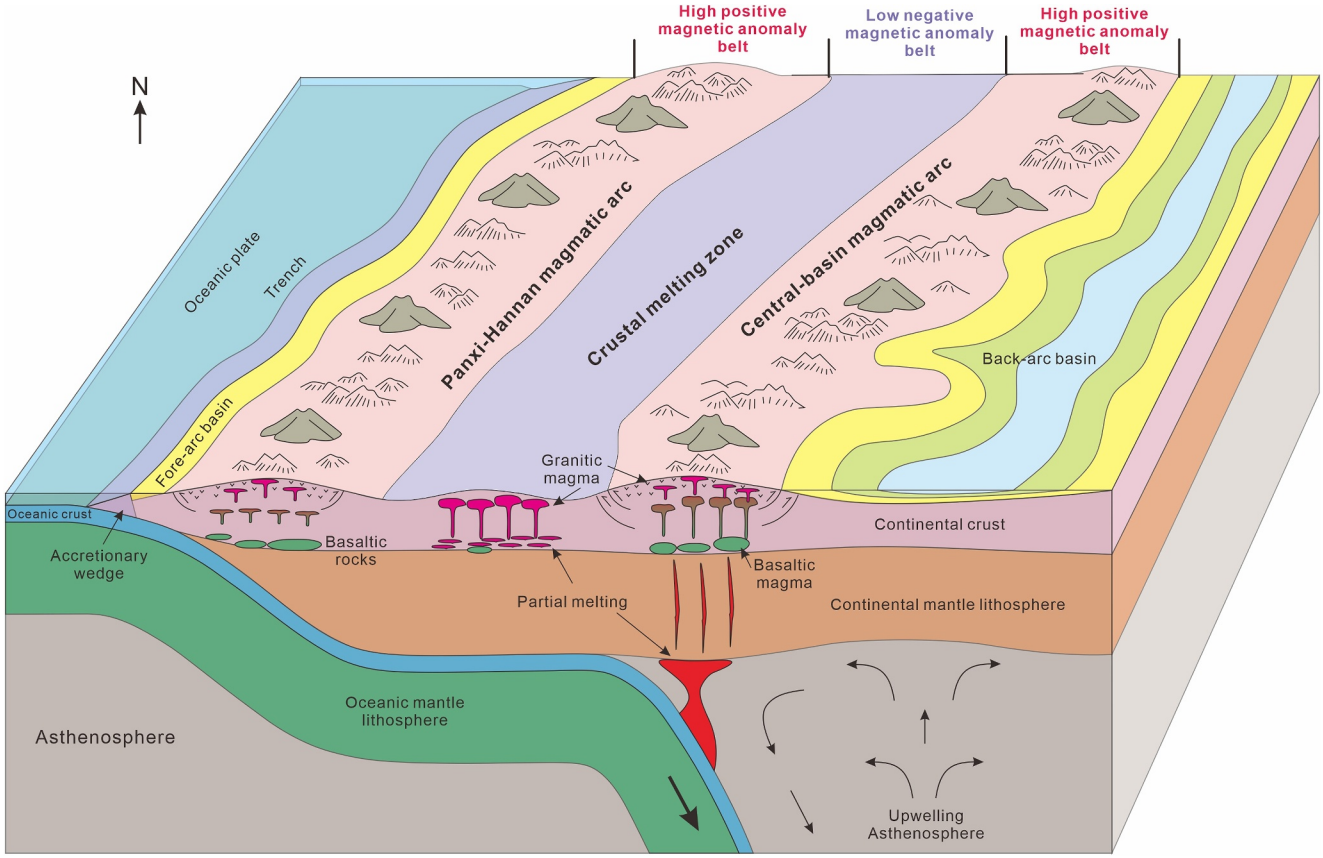

Figure 8. Schematic cartoon shows a long-distance arc migration during Tonian along the NW Yangtze Block. This model shows two Tonian juvenile continental arc systems that are contemporaneously present in the NW margin and interior of the Yangtze Block respectively (i.e., Panxi-Hannan and Central-basin magmatic arcs). A flat-slab subduction mechanism was inferred to generate such a broad continental arc system.

subduction direction, and (b) the SINOPROBE deep reflection profile across the Moho, which reveals eastward Tonian subduction relics beneath the central Sichuan Basin (Gao et al., 2016). On the other hand, the PHA, which includes a range of calc-alkaline plutonic and volcanic rocks, was conventionally considered as representative of the Tonian continental arc along west–northwest margin of the Yangtze Block (Zhao et al., 2019, 2021) (Figure 1b). However, some authors have identified more Tonian arc magmatic rocks beyond the PHA, in external regions such as the Bikou terrane (Gu et al., 2023; Xiao et al., 2007; Yan et al., 2003) and the West Qinling orogen (Gu et al., 2025a) (Figure 1b). These progresses lead to a redefinition of the NW Yangtze margin to the northwest of the PHA. Combined with our newly-acquired results, our calculations suggest that the Tonian arc magmatism extends at least ~400–900 km landward from the northwestern margin of the Yangtze Block. This distance encompasses a segment from Nanchong (i.e., the center of the PMAB within the basin) to the Longmenshan fold-thrust belt (LFB in Figure 1b, ~200 km), and another segment from the LFB to the NW margin of the Bikou terrane (BT in Figure 1b, ~200 km). Alternatively, a longer segment extends to Wushan (Figure 1b, potentially the further NW margin of the Yangtze Block, ~500 km). Such a wide continental arc system is comparable to modern Andes arc in Central Mexico, Peru, and Central Chile (Jordan et al., 1983; Liu & Currie, 2019; Manea et al., 2017) (~300–500 km), Late Cretaceous-Early Cenozoic western North American arc system (Axen et al., 2018; Carrapa et al., 2019; Coney & Reynolds, 1977; Fan & Carrapa, 2014) (~800–2,000 km), and Mesozoic South China arc system (Dai et al., 2020; Li & Li, 2007; Liu et al., 2021a, 2021b) (~1,300 km). These comparisons suggest that the long-distance arc migration in the NW Yangtze Block likely has been induced by flat-slab subduction (Figure 8). The flat-slab subduction model is also supported by following evidence. Firstly, a deep seismic reflection profile across the Sichuan Basin by Gao et al. (2016) has depicted the morphology of Neoproterozoic subducting slab relic to be low-angle (<30° to horizontal), consistent with flat-slab subduction geometries. Secondly, the flat-slab subduction could explain the lack of cold eclogites and

blueschists in the studied and worldwide early Neoproterozoic subduction zones (Brown et al., 2020), as the subducting slab was possibly hot and buoyant at that time.

On the other hand, this broad and ancient orogenic system archives significant crustal evolution processes, involving both juvenile crustal growth and the reworking of pre-existing crust, which had led to widespread formation of felsic igneous rocks in upper crust. The initial subsidence of cratonic basins, as exemplified by the Sichuan Basin of this study, may be driven by a series of orogeny-related processes, including uplift (thermal expansion), exhumation (orogeny), and subsequent thermal cooling. Additionally, this broad orogen was subject to long-timescale (>100 Myr) weathering as indicated by the borehole stratigraphic correlations (Figure 2a). The erosion products of the continental arcs may fertilize nearby sedimentary domains with wealthy nutrients, ultimately leading the formation of Tonian–Ediacaran sedimentary successions, hydrocarbon organic rocks and ultra-deep gas reservoirs in the Sichuan Basin.

6. Conclusion

Widespread Tonian (ca. 820–770 Ma) felsic igneous basements are identified beneath the Sichuan Basin in the interior of the Yangtze Block, South China. These felsic rocks exhibit different petrogenesis in different areas of the basin. The felsic rocks in observed high positive magnetic anomaly belt (PMAB) show juvenile geochemical signatures and were derived from trans-crustal differentiation or rapid partial melting of mantle-derived basaltic melts/rocks, while those in low-negative magnetic anomaly belt (NMAB) were possibly derived from partial melting of supracrustal sediments. The PMAB area records significant juvenile magmatism during Tonian period and its crust is associated with a fossil Tonian magmatic arc widely hidden beneath the basin. Our finding extends the circum-Yangtze Tonian continental arc system into the Yangtze interior, while such a long-distance arc migration is interpreted as a result of the flat-slab subduction process. This broad and ancient orogenic system played a significant role in crustal growth and recycling of the Yangtze Block.

Conflict of Interest

The authors declare no conflicts of interest relevant to this study.

Data Availability Statement

The Supporting Information S1, S2 is available at Gu et al. (2025b). The Supporting Information S1 Tables are available at Gu et al. (2025c). The Supporting Information S1 includes two parts: (a) Supporting Information S1 file contains Figure S1 to S9 in Supporting Information S1; (b) Tables S1 and S2 in Supporting Information S1 separately as Excel files, showing all analytical data.

Acknowledgments
This work was supported by the Science and Technology Major Project of PetroChina (No. 2023ZZ0201), the National Science and Technology Major Project of the Ministry of Science and Technology of China (No. 2016ZX05004005-001), the Science and Technology Project of RIPED (No. YGJ2023-01), and the National Natural Science Foundation of China (Nos. 42025202 and 42202053). We are very grateful for the thoughtful and constructive reviews provided by Editor Mark Dekkers, the associate editor, Wenjiao Xiao, and an anonymous reviewer, all of which significantly improved this paper. We also thank Mark Dekkers for his expeditious editorial handling.

References

Axen, G. J., Wijk, J. W., & Currie, C. A. (2018). Basal continental mantle lithosphere displaced by flat-slab subduction. *Nature Geoscience*, *11*(12), 961–964. https://doi.org/10.1038/s41561-018-0263-9

Brown, M., Kirkland, C. L., & Johnson, T. E. (2020). Evolution of geodynamics since the archean: Significant change at the dawn of the phanerozoic. *Geology*, *48*(5), 488–492. https://doi.org/10.1130/G47417.1

Cao, W., Lee, C. T. A., & Lackey, J. S. (2017). Episodic nature of continental arc activity since 750 Ma: A global compilation. *Earth and Planetary Science Letters*, *461*, 85–95. https://doi.org/10.1016/j.epsl.2016.12.044

Carrapa, B., DeCelles, P. G., & Romero, M. (2019). Early inception of the laramide orogeny in southwestern Montana and northern Wyoming: Implications for models of flat-slab subduction. *Journal of Geophysical Research: Solid Earth*, *124*(2), 2102–2123. https://doi.org/10.1029/2018JB016888

Cawood, P. A., & Hawkesworth, C. J. (2014). Earth's middle age. *Geology*, *42*(6), 503–506. https://doi.org/10.1130/G35402.1

Cawood, P. A., Zhao, G., Yao, J., Wang, W., Xu, Y., & Wang, Y. (2018). Reconstructing South China in phanerozoic and precambrian supercontinents. *Earth-Science Reviews*, *186*, 173–194. https://doi.org/10.1016/j.earscirev.2017.06.001

Chen, C. S., Qin, S. F., Wang, Y. P., Holland, G., Wynn, P., Zhong, W. X., & Zhou, Z. (2022). High temperature methane emissions from Large Igneous Provinces as contributors to late Permian mass extinctions. *Nature Communications*, *13*(1), 6893. https://doi.org/10.1038/s41467-022-34645-3

Chung, S. L., & Jahn, B. M. (1995). Plume-lithosphere interaction in generation of the Emeishan flood basalts at the Permian-Triassic boundary. *Geology*, *23*(10), 889–892. https://doi.org/10.1130/0091-7613(1995)023<0889:pliigo>2.3.co;2

Coble, M. A., Vazquez, J. A., Barth, A. P., Wooden, J., Burns, D., Kylander-Clark, A., et al. (2018). Trace element characterisation of MAD-559 zircon reference material for ion microprobe analysis. *Geostandards and Geoanalytical Research*, *42*(4), 481–497. https://doi.org/10.1111/ggr.12238

Coney, P. J., & Reynolds, S. J. (1977). Cordilleran Benioff zones. *Nature*, *270*(5636), 403–406. https://doi.org/10.1038/270403a0

Dai, L. M., Wang, L. L., Lou, D., Li, Z. H., Dong, D., Ma, F. F., et al. (2020). Slab rollback versus delamination: Contrasting fates of flat-slab subduction and implications for South China evolution in the Mesozoic. *Journal of Geophysical Research: Solid Earth*, *125*(4), e2019JB019164. https://doi.org/10.1029/2019JB019164

Dong, Y. P., Hui, B., Sun, S. S., He, D. F., Sun, J. P., Zhang, F. F., et al. (2024). Neoproterozoic tectonic evolution and proto-basin of the Yangtze Block, China. *Earth-Science Reviews*, *249*, 104669. https://doi.org/10.1016/j.earscirev.2023.104669

Druschke, P., Hanson, A. D., Yan, Q., Wang, Z., & Wang, T. (2006). Stratigraphic and U–Pb SHRIMP detrital zircon evidence for a Neoproterozoic continental arc, Central China: Rodinia implications. *The Journal of Geology*, *114*(5), 627–636. https://doi.org/10.1086/506162

Ducea, M. N., Saleeby, J. B., & Bergantz, G. (2015). The architecture, chemistry, and evolution of continental magmatic arcs. *Annual Review of Earth and Planetary Sciences*, *43*(1), 299–331. https://doi.org/10.1146/annurev-earth-060614-105049

Ducea, M. N., & Chapman, A. D. (2018). Sub-magmatic arc underplating by trench and forearc materials in shallow subduction systems; A geologic perspective and implications. *Earth-Science Reviews*, *185*, 763–779. https://doi.org/10.1016/j.earscirev.2018.08.001

Fan, M. J., & Carrapa, B. (2014). Late Cretaceous–early Eocene Laramide uplift, exhumation, and basin subsidence in Wyoming: Crustal responses to flat slab subduction. *Tectonics*, *33*(4), 509–529. https://doi.org/10.1002/2012TC003221

Gao, R., Chen, C., Wang, H. Y., Lu, Z. W., Brown, L., Dong, S. W., et al. (2016). SINOPROBE deep reflection profile reveals a Neo-Proterozoic subduction zone beneath Sichuan Basin. *Earth and Planetary Science Letters*, *454*, 86–91. https://doi.org/10.1016/j.epsl.2016.08.030

Garrett, S. W. (1990). Interpretation of reconnaissance gravity and aeromagnetic surveys of the Antarctic Peninsula. *Journal of Geophysical Research*, *95*(B5), 6759–6777. https://doi.org/10.1029/JB095iB05p06759

Ge, R. F., Wilde, S. A., Zhu, W. B., & Wang, X. L. (2023). Earth's early continental crust formed from wet and oxidizing arc magmas. *Nature*, *623*(7986), 334–339. https://doi.org/10.1038/s41586-023-06552-0

Grimes, C. B., Wooden, J. L., Cheadle, M. J., & John, B. E. (2015). "Fingerprinting" tectono-magmatic provenance using trace elements in igneous zircon. *Contributions to Mineralogy and Petrology*, *170*(46), 1–26. https://doi.org/10.1007/s00410-015-1199-3

Gu, Z. D., Jian, X., Liu, G. X., Fu, H. J., Shen, X. T., Zhai, X. F., & Jiang, H. (2025a). The Tonian sedimentary records in the southwestern West Qinling orogen, central China, reveal an active margin setting. *Precambrian Research*, *418*, 107692. https://doi.org/10.1016/j.precamres.2025.107692

Gu, Z. D., Jian, X., Liu, G. X., Shen, X. T., Fu, H. J., Zhai, X. F., & Jiang, H. (2023). Age, provenance and tectonic setting of the Tonian-Cryogenian clastic successions in the northwest Bikou terrane, NW Yangtze Block, Central China. *Precambrian Research*, *397*, 107197. https://doi.org/10.1016/j.precamres.2023.107197

Gu, Z. D., Li, J. Y., Wang, X. L., Xu, Y., & Zhai, X. F. (2025b). Supporting information for "A ~700-km-long fossil Tonian Magmatic Arc Belt hidden within the Yangtze block's interior, South China" submitted to JGR-solid earth. *Figshare*. [Figure]. https://doi.org/10.6084/m9.figshare.28523075.v3

Gu, Z. D., Li, J. Y., Wang, X. L., Xu, Y., & Zhai, X. F. (2025c). Supplementary Tables for "A ~700-km-long fossil Tonian Magmatic Arc Belt hidden within the Yangtze block's interior, South China" submitted to JGR-solid earth [Dataset]. *figshare*. https://doi.org/10.6084/m9.figshare.28523411.v3

Gu, Z. D., Lonergan, L., Zhai, X. F., Zhang, B. M., & Lu, W. H. (2021). The formation of the Sichuan Basin, South China, during the late Ediacaran to early Cambrian. *Basin Research*, *33*(4), 1255–2357. https://doi.org/10.1111/bre.12559

Gu, Z. D., & Wang, Z. C. (2014). The discovery of neoproterozoic extensional structures and its significance for gas exploration in the central Sichuan block, Sichuan Basin, South China. *Science China Earth Sciences*, *44*(11), 2210–2220. https://doi.org/10.1007/s11430-014-4961-x

Gu, Z. D., Zhang, W., & Yuan, M. (2014). Zircon SHRIMP U-Pb dating of basal granite and its geological significance in Weiyuan area of Sichuan Basin. *Chinese Journal of Geology*, *49*(1), 202–213. Chinese in English Abstract. https://doi.org/10.3969/j.issn.0563-5020.2014.01.015

Guan, S. W., Wu, L., Ren, R., Zhu, G. Y., Peng, Z. Q., Zhao, W. T., & Li, J. (2017). Distribution and petroleum prospect of Precambrian rifts in the main cratons, China. *Acta Petrolei Sinica*, *38*, 9–22. https://doi.org/10.7623/syxb201701002

He, D. F., Li, D., Fan, C., & Yang, X. F. (2013). Geochronology, geochemistry and tectonostratigraphy of carboniferous strata of the deepest well Moshen-1 in the Junggar Basin, northwest China: Insights into the continental growth of central Asia. *Gondwana Research*, *24*(2), 560–577. https://doi.org/10.1016/j.gr.2012.10.015

Jacob, J. B., & Moyen, J. F. (2021). Granite and related rocks. In D. Alderton & S. A. Elias (Eds.), *Encyclopedia of Geology* (2nd ed., pp. 170–183). Academic Press.

Jagoutz, O., & Kelemen, P. B. (2015). Role of arc processes in the formation of continental crust. *Annual Review of Earth and Planetary Sciences*, *43*(1), 363–404. https://doi.org/10.1146/annurev-earth-040809-152345

Jordan, T. E., Isacks, B. L., Allmendinger, R. W., Brewer, J. A., Ramos, V. A., & Ando, C. J. (1983). Andean tectonics related to geometry of subducted Nazca plate. *Geological Society of America Bulletin*, *94*, 341–361. https://doi.org/10.1130/0016–7606(1984)95<877:atrtgo>2.0.CO;2

Kemp, A. I. S., Hawkesworth, C. J., Foster, G. L., Paterson, B. A., Woodhead, J. D., Hergt, J. M., et al. (2007). Magmatic and crustal differentiation history of granitic rocks from Hf-O isotopes in zircon. *Science*, *315*(5814), 980–983. https://doi.org/10.1126/science.1136154

Korsch, R. J., Mai, H. Z., Sun, Z. C., & Gorter, J. D. (1991). The Sichuan Basin, southwest China: A late proterozoic (Sinian) petroleum province. *Precambrian Research*, *54*(1), 45–63. https://doi.org/10.1016/0301-9268(91)90068-I

Lee, C. T. A., Thurner, S., Paterson, S., & Cao, W. (2015). The rise and fall of continental arcs: Interplays between magmatism, uplift, weathering, and climate. *Earth and Planetary Science Letters*, *425*, 105–119. https://doi.org/10.1016/j.epsl.2015.05.045

Li, J. Y., Tang, M., Lee, C. A., Wang, X. L., Gu, Z. D., Xia, X. P., et al. (2021). Rapid endogenic rock recycling in magmatic arcs. *Nature Communications*, *12*(1), 3533. https://doi.org/10.1038/s41467-021-23797-3

Li, J. Y., Wang, X. L., Cawood, P. A., Gu, Z. D., & Guan, Y. (2024). Neoproterozoic low-T/P metamorphism in the Yangtze Block manifests a long-lived subduction girdle around Rodinia. *Earth and Planetary Science Letters*, *634*, 118678. https://doi.org/10.1016/j.epsl.2024.118678

Li, J. Y., Wang, X. L., & Gu, Z. D. (2018). Early neoproterozoic arc magmatism of the tongmuliang group on the northwestern margin of the Yangtze block: Implications for Rodinia assembly. *Precambrian Research*, *309*, 181–197. https://doi.org/10.1016/j.precamres.2017.04.040

Li, X. H., Tang, G. Q., Gong, B., Yang, Y. H., Hou, K. J., Hu, Z. C., et al. (2013). Qinghu zircon: A working reference for microbeam analysis of U-Pb age and Hf and O isotopes. *Chinese Science Bulletin*, *58*(36), 4647–4654. https://doi.org/10.1007/s11434-013-5932-x

Li, Z. X., & Li, X. H. (2007). Formation of the 1300-km-wide intracontinental orogen and postorogenic magmatic province in Mesozoic South China: A flat-slab subduction model. *Geology*, *35*(2), 179–182. https://doi.org/10.1130/G23193A.1

Lin, S. F., Wang, L. J., Xiao, W. J., Xing, G. F., Niu, Z. J., Zhao, X. L., et al. (2023). *The early paleozoic Wuyi–Yunkai orogeny in South China: A collisional orogeny with a major lag in time between onset of collision and peak metamorphism in subducted continental crust*. (Vol. 542, pp. 619–641). Geological Society, London, Special Publication. https://doi.org/10.1144/SP542-2023-6

Liu, L., Liu, L. J., & Xu, Y. G. (2021). Mesozoic intraplate tectonism of East Asia due to flat subduction of a composite terrane slab. *Earth-Science Reviews*, *214*, 103505. https://doi.org/10.1016/j.earscirev.2021.103505

Liu, S. G., Yang, Y., Deng, B., Zhong, Y., Wen, L., Sun, W., et al. (2021). Tectonic evolution of the Sichuan Basin, southwest China. *Earth-Science Reviews*, *213*, 103470. https://doi.org/10.1016/j.earscirev.2020.103470

Liu, X. W., & Currie, C. (2019). Influence of upper plate structure on flat-slab depth: Numerical modeling of subduction dynamics. *Journal of Geophysical Research: Solid Earth*, *124*(12), 13150–13167. https://doi.org/10.1029/2019JB018653

Manea, V. C., Manea, M., Ferrari, L., Orozco-Esquivel, T., Valenzuela, R. W., Husker, A., & Kostoglodov, V. (2017). A review of the geodynamic evolution of flat slab subduction in Mexico, Peru, and Chile. *Tectonophysics*, *695*, 27–52. https://doi.org/10.1016/j.tecto.2016.11.037

Profeta, L., Ducea, M. N., Chapman, J. B., Paterson, S. R., Gonzales, S. M. H., Kirsch, M., et al. (2015). Quantifying crustal thickness over time in magmatic arcs. *Scientific Reports*, *5*(1), 17786. https://doi.org/10.1038/srep17786

Roberts, N. M. W., Yakymchuk, C., Spencer, C. J., Keller, C. B., & Tapster, S. R. (2024). Revisiting the discrimination and distribution of S-type granites from zircon trace element composition. *Earth and Planetary Science Letters*, *633*, 118638. https://doi.org/10.1016/j.epsl.2024.118638

Shu, L. S., Yao, J. L., Wang, B., Faure, M., Charvet, J., & Chen, Y. (2021). Neoproterozoic plate tectonic process and Phanerozoic geodynamic evolution of the South China Block. *Earth-Science Reviews*, *216*, 103596. https://doi.org/10.1016/j.earscirev.2021.103596

Stern, R. J. (2018). The evolution of plate tectonics. *Philosophical Transactions of the Royal Society A: Mathematical, Physical and Engineering Sciences*, *376*(2132), 20170406. https://doi.org/10.1098/rsta.2017.0406

Stern, R. J. (2020). The Mesoproterozoic single-lid tectonic episode: Prelude to modern plate tectonics. *Geological Society of America Today*, *30*(12), 4–10. https://doi.org/10.1130/GSATG480A.1.CC-BY-NC

Tanaka, A., Okubo, Y., & Matsubayashi, O. (1999). Curie point depth based on spectrum analysis of the magnetic anomaly data in East and Southeast Asia. *Tectonophysics*, *306*(3–4), 461–470. https://doi.org/10.1016/S0040-1951(99)00072-4

Tang, M., Ji, W. Q., Chu, X., Wu, A., & Chen, C. (2021). Reconstructing crustal thickness evolution from europium anomalies in detrital zircons. *Geology*, *49*(1), 76–80. https://doi.org/10.1130/G47745.1

Valley, J. W. (2003). Oxygen isotopes in zircon. In *Reviews in Mineralogy and Geochemistry* (Eds.) J. M. Hanchar & P. W. O. Hoskin, (Vol. 53, pp. 343–385). https://doi.org/10.2113/0530343

Wang, E., & Meng, Q. (2009). Mesozoic and Cenozoic tectonic evolution of the Longmenshan fault belt. *Science in China - Series D: Earth Sciences*, *52*(5), 579–592. https://doi.org/10.1007/s11430-009-0053-8

Wang, L. J., Lin, S. F., & Xiao, W. J. (2023). Yangtze and Cathaysia blocks of South China: Their separate positions in Gondwana until early Paleozoic juxtaposition. *Geology*, *51*(8), 723–727. https://doi.org/10.1130/G51362.1

Wang, M. X., Nebel, O., & Wang, C. Y. (2016). The flaw in the crustal "zircon archive": Mixed Hf isotope signatures record progressive contamination of late-stage liquid in mafic–ultramafic layered intrusions. *Journal of Petrology*, *57*(1), 27–52. https://doi.org/10.1093/petrology/egv072

Wang, X. L., Zhou, J. C., Griffin, W. L., Zhao, G. C., Yu, J. H., Qiu, J. S., et al. (2014). Geochemical zonation across a Neoproterozoic orogenic belt: Isotopic evidence from granitoids and metasedimentary rocks of the Jiangnan Orogen, China. *Precambrian Research*, *242*, 154–171. https://doi.org/10.1016/j.precamres.2013.12.023

Woodhead, J. D., & Hergt, J. M. (2005). A preliminar appraisal of seven natural zircon reference materials for in situ Hf isotope determination. *Geostandards and Geoanalytical Research*, *29*(2), 183–195. https://doi.org/10.1111/j.1751-908x.2005.tb00891.x

Wu, P., Wu, Y. B., Zhang, S. B., Zheng, Y. F., Li, L., Gao, Y., et al. (2024). Revisiting neoproterozoic tectono-magmatic evolution of the northern margin of the Yangtze block, South China. *Earth-Science Reviews*, *255*, 104825. https://doi.org/10.1016/j.earscirev.2024.104825

Wu, P., Zhang, S. B., Li, Z. X., Wu, Y. B., & Zheng, Y. F. (2023). Secular change in the nature of mantle and tectonic evolution of northwestern margin of the Yangtze Block during Neoproterozoic: Constraints from the mafic intrusions and associated granitoids of the Hannan and Xiaomoling complexes. *Precambrian Research*, *393*, 107094. https://doi.org/10.1016/j.precamres.2023.107094

Xiao, L., Zhang, H. F., Ni, P. Z., Xiang, H., & Liu, X. M. (2007). LA-ICP-MS U–Pb zircon geochronology of early neoproterozoic mafic-intermediate intrusions from NW margin of the Yangtze block, South China: Implication for tectonic evolution. *Precambrian Research*, *154*(3–4), 221–235. https://doi.org/10.1016/j.precamres.2006.12.013

Xiao, W. J., Windley, B. F., Han, C. M., Liu, W., Wan, B., Zhang, J. E., et al. (2018). Late Paleozoic to early Triassic multiple roll-back and oroclinal bending of the Mongolia collage in Central Asia. *Earth Science Review*, *186*, 94–128. https://doi.org/10.1016/j.earscirev.2017.09.020

Xiong, F. H., Zhong, H. T., Huang, H., Liu, X. C., & Hou, M. C. (2023). Petrogenetic and tectonic implications of Neoproterozoic igneous rocks from the western Yangtze Block, South China. *Precambrian Research*, *387*, 106977. https://doi.org/10.1016/j.precamres.2023.106977

Xu, Y., Chung, S. L., Jahn, B. M., & Wu, G. (2001). Petrologic and geochemical constraints on the petrogenesis of Permian–Triassic Emeishan flood basalts in southwestern China. *Lithos*, *58*(3–4), 145–168. https://doi.org/10.1016/s0024-4937(01)00055-x

Xu, Y. G., He, B., Huang, X. L., Luo, Z. Y., Chung, S. L., Xiao, L., et al. (2007). Identification of mantle plumes in the emeishan large igneous province. *Episodes*, *30*(1), 32–42. https://doi.org/10.18814/epiiugs/2007/v30i1/005

Yan, Q. R., Wang, Z. Q., Hanson, A. D., Druschke, P. A., Yan, Z., Liu, D. Y., et al. (2003). SHRIMP age and geochemistry of the Bikou volcanic terrane: Implications for neoproterozoic tectonics on the northern margin of the Yangtze craton. *Acta Geologica Sinica*, *77*(4), 479–490. https://doi.org/10.1111/j.1755-6724.2003.tb00128.x

Yang, X. S., Tian, X. B., Windley, B. F., Zhao, L., Lu, Y. F., Yuan, H. Y., & Xiao, W. J. (2022). The role of multiple trapped oceanic basins in continental growth: Seismic evidence from the southern Altaids. *Geophysical Research Letter*, *49*(11), e2022GL098548. https://doi.org/10.1029/2022gl098548

Yang, Z. R., Wang, X. J., Feng, X. K., Ji, X. W., Xu, H., & Li, M. Y. (2014). Geological research and significance of a rift valley in the Presinian period in central Sichuan Basin. *Natural Gas Industry*, *34*(3), 80–85. https://doi.org/10.3787/j.issn.1000-0976.2014.03.013

Yao, J. L., Cawood, P. A., Shu, L. S., & Zhao, G. C. (2019). Jiangnan orogen, South China: A ~970–820 Ma Rodinia margin accretionary belt. *Earth-Science Reviews*, *196*, 102872. https://doi.org/10.1016/j.earscirev.2019.05.016

Zhao, G., & Cawood, P. A. (2012). Precambrian geology of China. *Precambrian Research*, *222-223*, 13–54. https://doi.org/10.1016/j.precamres.2012.09.017

Zhao, J. H., Li, Q. W., Liu, H., & Wang, W. (2018). Neoproterozoic magmatism in the western and northern margins of the Yangtze Block (South China) controlled by slab subduction and subduction-transform-edge-propagator. *Earth-Science Reviews*, *187*, 1–18. https://doi.org/10.1016/j.earscirev.2018.10.004

Zhao, J. H., Nebel, O., & Johnson, T. E. (2021). Formation and evolution of a Neoproterozoic continental magmatic arc. *Journal of Petrology*, *62*(8), egab029. https://doi.org/10.1093/petrology/egab029

Zhao, J. H., & Zhou, M. F. (2009). Secular evolution of the Neoproterozoic lithospheric mantle underneath the northern margin of the Yangtze Block, South China. *Lithos*, *107*(3–4), 152–168. https://doi.org/10.1016/j.lithos.2008.09.017

Zhao, J. H., Zhou, M. F., Wu, Y. B., Zheng, J. P., & Wang, W. (2019). Coupled evolution of Neoproterozoic arc mafic magmatism and mantle wedge in the western margin of the South China Craton. *Contributions to Mineralogy and Petrology*, *174*(4), 36. https://doi.org/10.1007/s00410-019-1573-7

Zhao, J. H., Zhou, M. F., Yan, D. P., Zheng, J. P., & Li, J. W. (2011). Reappraisal of the ages of neoproterozoic strata in South China: No connection with the Grenvillian orogeny. *Geology*, *39*(4), 299–302. https://doi.org/10.1130/g31701.1

Zhou, M. F., Kennedy, A. K., Sun, M., Malpas, J., & Lesher, C. M. (2002). Neoproterozoic arc-Related mafic intrusions along the northern margin of SouthSouth China: Implications for the accretion of Rodinia. *The Journal of Geology*, *110*(5), 611–618. https://doi.org/10.1086/341762

Zhou, M. F., Yan, D. P., Kennedy, A. K., Li, Y., & Ding, J. (2002). SHRIMP U–Pb zircon geochronological and geochemical evidence for Neoproterozoic arc-magmatism along the western margin of the Yangtze Block, South China. *Earth and Planetary Science Letters*, *196*(1–2), 51–67. https://doi.org/10.1016/s0012-821x(01)00595-7